Journal of
Applied Crystallography
ISSN 0021-8898
Editor: **Anke R. Pyzalla**

Pressure-induced high-density amorphous ice in protein crystals

Chae Un Kim, Yi-Fan Chen, Mark W. Tate and Sol M. Gruner

J. Appl. Cryst. (2008). **41**, 1–7

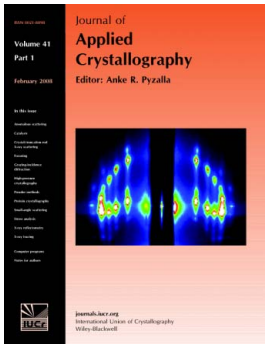

Journal of
Applied Crystallography
ISSN 0021-8898

Received 12 July 2007
Accepted 4 October 2007

Pressure-induced high-density amorphous ice in protein crystals

Chae Un Kim,[a,b] Yi-Fan Chen,[a,b] Mark W. Tate[c,d] and Sol M. Gruner[a,b,c,d]*

[a]Field of Biophysics, Cornell University, Ithaca, NY 14853, USA, [b]Cornell High Energy Synchrotron Source (CHESS), Ithaca, NY 14853, USA, [c]Laboratory of Atomic and Solid State Physics, Cornell University, Ithaca, NY 14853, USA, and [d]Physics Department, Cornell University, Ithaca, NY 14853, USA. Correspondence e-mail: smg26@cornell.edu

Crystal cryocooling has been used in X-ray protein crystallography to mitigate radiation damage during diffraction data collection. However, cryocooling typically increases crystal mosaicity and often requires a time-consuming search for cryoprotectants. A recently developed high-pressure cryocooling method reduces crystal damage relative to traditional cryocooling procedures and eases or eliminates the need to screen for cryoprotectants. It has been proposed that the formation of high-density amorphous (HDA) ice within the protein crystal is responsible for the excellent diffraction quality of the high-pressure cryocooled crystals. This paper reports X-ray data that confirm the presence of HDA ice in the high-pressure cryocooled protein crystallization solution and protein crystals analyzed at ambient pressure. Diffuse scattering with a spacing characteristic of HDA ice is seen at low temperatures. This scattering then becomes characteristic successively to low-density amorphous, cubic and hexagonal ice phases as the temperature is gradually raised from 80 to 230 K, and seems to be highly correlated with the diffraction quality of crystals.

1. Introduction

In X-ray protein crystallography, a typical protein crystal at room temperature only survives a fraction of the total X-ray dose needed for a complete high-resolution data set before it is destroyed by X-ray radiation damage (Ravelli & Garman, 2006). Over the past two decades, cryocrystallography techniques, whereby a protein crystal is flash-cryocooled and the crystal diffraction data are collected at cryogenic temperatures, have played a key role in mitigating radiation damage (Garman & Schneider, 1997). However, crystal cryocooling typically requires finding suitable cryoprotectants, which is not always successful, and most commonly results in crystals with significantly increased mosaic spreads (Garman & Owen, 2006).

An alternative crystal cryocooling method, high-pressure cryocooling, was developed by Kim *et al.* (2005), where use of penetrating cryoprotectants could be avoided by cryocooling protein crystals in helium gas at high pressures. This method was tested with various protein crystals and commonly resulted in exceptionally high-quality crystal diffraction. It also has proven useful in improving diffraction from protein ligand complexes. For example, it was successfully used in the study of the RCK domain of the KtrAB K^+ transporter, not only to obtain excellent diffraction but also to limit the perturbation of the ligand binding site by cryoprotectants (Albright *et al.*, 2006). More recently, the high-pressure cryocooling method was extended to crystal diffraction phasing by the incorporation of heavy noble gases, krypton and xenon (Kim *et al.*, 2006, 2007). It was also shown that the method can be used to cryoprotect an entire capillary sample consisting of crystals and crystallization solution in a thick-walled polycarbonate capillary (Kim *et al.*, 2007).

Kim *et al.* (2005) proposed a mechanism for high-pressure cryocooling, involving the formation of high-density amorphous (HDA) ice, for the solution internal to the protein crystals. In contrast to low-density amorphous (LDA) ice, which forms at ambient pressure by hyperquenched cryocooling, with a density of 0.94 g cm^{-3} at 77 K and 0.1 MPa (Ghormley & Hochanadel, 1971), HDA ice has significantly higher density: 1.17 g cm^{-3} at 77 K, 0.1 MPa (Mishima *et al.*, 1984). The volume expansion of water upon the formation of LDA has been suggested as the cause for the increased crystal mosaicity observed with conventional cryocooling (Kriminski *et al.*, 2002; Juers & Matthews, 2004). It has been suggested that the density difference between LDA and HDA may account for the lower mosaicity observed with high-pressure cryocooling (Kim *et al.*, 2005).

Conventionally, HDA ice of pure water has been prepared by pressure-induced amorphization in which hexagonal ice at liquid-nitrogen temperature is subject to high pressure of 1.2–2.0 GPa and undergoes a collapse-transition to HDA ice (see Mishima & Stanley, 1998, for a review). In contrast, high-pressure cryocooling of protein crystals has been performed at considerably lower pressures, in the region of 100–200 MPa, albeit not with pure water. Therefore, it has been of consid-

erable interest to see if HDA ice forms inside protein crystals by high-pressure cryocooling.

Below, we describe the use of X-ray diffraction to study water phases in both the solution used for protein crystallization and in protein crystals prepared by high-pressure cryocooling. The results support the existence of HDA ice produced by high-pressure cryocooling both in bulk solution and within protein crystals. As each sample was warmed from 80 to 270 K, phase transitions from HDA ice to LDA ice, cubic ice and hexagonal ice could be observed, which correlated with the diffraction quality of the crystals.

2. Experimental details

2.1. Sample preparation

The crystallization solution of 0.9 *M* sodium potassium tartrate in pure water, which was used in the preparation of the thaumatin crystals, was used without thaumatin protein for the bulk-solution study. The sample, in a capillary, was prepared by centrifuging the solution for 20 s to the bottom of a glass X-ray capillary (catalog No. 05-SG, Charles Supper Company, Natick, MA) having a length of 15 mm, a diameter of 0.5 mm and a wall thickness of 10 µm. A MicroTube (catalog No. HR4-917, Hampton Research, Laguna Niguel, CA) of 12 mm length was press-fitted into the open end of the capillary to facilitate sample manipulation.

Lyophilized thaumatin powder from *Thaumatococcus daniell* (catalog No. T7638, Sigma, Saint Louis, MO) was used for crystallization without further purification. Crystals were grown at room temperature by the hanging-drop method with 25 mg ml^{-1} thaumatin solution in 50 m*M* HEPES buffer at pH 7 and crystallization solution containing 0.9 *M* sodium potassium tartrate as a precipitant (modified from Ko *et al.*, 1994). The crystal space group was determined to be $P4_12_12$, having a solvent content of ∼55%.

Glucose isomerase from *Streptomyces rubiginosus* (catalog No. HR7-102, Hampton Research, Laguna Niguel, CA) was dialyzed against pure water before crystallization. Crystals were grown by the hanging-drop method by mixing a reservoir solution containing 1.15 *M* ammonium sulfate, 1 m*M* magnesium sulfate and 10 m*M* HEPES pH 7.5 with 25 mg ml^{-1} protein solution in pure water (modified from Carrell *et al.*, 1989). The crystal space group was determined to be *I*222, having a solvent content of ∼55%.

Lyophilized porcine pancreas elastase (catalog No. 20929, SERVA, Heidelberg, Germany) was used for crystallization without further purification. Crystals were grown by the hanging-drop method by mixing a reservoir solution containing 30 m*M* sodium sulfate and 50 m*M* sodium acetate pH 5.0 with a 25 mg ml^{-1} protein solution in pure water (modified from Shotton *et al.*, 1968). The crystal space group was determined to be $P2_12_12_1$, having a solvent content of ∼40%.

Prior to high-pressure cryocooling, protein crystals were mounted on 0.3–0.4 mm mounted-cryoloops. To avoid crystal dehydration, the crystals were coated with NVH oil (catalog No. HR3-611, Hampton Research). Excess crystallization solution around crystals was carefully removed during the oil-coating process by swishing the crystals back and forth in the oil. The amount of crystallization solution surrounding a protein crystal was negligible relative to the amount of solvent inside the crystal.

2.2. High-pressure cryocooling

Samples were high-pressure cryocooled as described by Kim *et al.* (2005). Briefly, samples were loaded into the high-pressure cryocooling apparatus, which was then pressurized with helium gas to 200 MPa at ambient temperature. Once at high pressure, the samples were allowed to fall into a zone at liquid-nitrogen temperature. Helium pressure was then released. Thereafter samples were handled/stored at ambient pressure and near liquid-nitrogen temperatures prior to X-ray diffraction measurements.

2.3. X-ray diffraction measurement

The X-ray diffraction data were collected at macromolecular crystallography stations A1 (λ = 0.9771 Å, ADSC Quantum 210 CCD detector, beam size of 100 µm) and F1 (λ = 0.9179 Å, ADSC Quantum 270 CCD detector, beam size of 100 µm) at the Cornell High Energy Synchrotron Source (CHESS). To prevent sample warming, a cryotong (Hampton Research) was used to transfer samples rapidly from liquid nitrogen to a goniometer. During data collection, samples were kept cold under a flow of cryogenic nitrogen gas from a Cryostream 700 series cryocooler from Oxford Cryosystems (Devens, MA). During the warming studies, sample temperature was increased at the rate of 2 K min^{-1}. After reaching a desired temperature, samples were left at the temperature for 5 to 10 min for sample equilibration. The X-ray diffraction data of the crystallization solution were collected with temperature steps of 0.5 to 10 K, and the data of the protein crystals were collected with steps of 2 to 10 K, with the smaller temperature steps taken in the vicinity of the phase transition. To obtain the unit-cell parameters and crystal mosaicity, five consecutive images were collected at each temperature, with an oscillation angle of 1° starting at the same crystal orientation. The X-ray exposure time was 15–30 s for the solution samples and 3–5 s for the protein crystal samples. The magnitude of the scattering vector **Q** is given by $Q = 4\pi\sin(\theta)/\lambda$, where λ is the X-ray wavelength and 2θ is the angle between the incident beam and the diffracted X-rays. The corresponding d spacing in real space is given by $d = 2\pi/Q$.

2.4. Data analysis

The diffraction from the protein crystals consists of Bragg peaks from the protein molecules in the crystal superimposed on the diffuse rings arising from the oil external to the crystal and water internal to the crystal. Recall that care was taken to remove most of the water external to the crystal during the oil-coating step. The underlying diffuse diffraction was isolated from the Bragg spots by applying a custom polar-coordinate median filter to the intensity values of the image. Median

filters that are routinely found in image-processing packages replace each pixel value in an image with the median value in a rectangular region centered on that pixel. In contrast, the polar-coordinate median filter replaces each pixel value with the median value of all pixels having the same scattering-vector magnitude, Q. The sample-to-detector distance was calibrated based on the reported Bragg peaks of the hexagonal ice (Blackman & Lisgarten, 1957).

Peak positions for the broad diffraction of amorphous ice from the pressure-cryocooled crystallization solution were determined by fitting a quadratic function in the vicinity of the maxima. The diffuse scattering from the amorphous ice phases within the protein crystal samples was found to be weaker than the nearby scattering peak from the oil used to coat the crystal. The oil and ice peaks, plus a second amorphous ice peak were fit to three Voigt functions plus a linear background. This choice of functions was used simply because it readily fits the experimental diffraction profile. The width and position of the cubic ice peaks were fit using Gaussian line shapes on a background composed of the Voigt functions used for the amorphous scattering described above.

Unit-cell parameters and crystal mosaicity at each temperature were refined by processing the five consecutive 1° oscillation images with *HKL2000* (Otwinowski & Minor, 1997). No corrections were made for beamline divergence (∼1 mrad in the horizontal), since the crystals quoted here have mosaicities of ∼5 mrad or more, so actual mosaicity improvements may be slightly better than stated.

3. Results and discussion

3.1. High-pressure cryocooled crystallization solution

X-ray diffraction measurements were conducted on a high-pressure cryocooled sample consisting of the bulk protein crystallization solution in the absence of protein. Figs. 1(*a*) and 2(*a*) show the scattering from this crystallization solution as temperature was increased. The position of the innermost peak of the ice scattering is shown from 80 to 170 K in Fig. 3. This peak was at Q = 2.10 Å^{-1} (d = 2.99 Å) at 80 K, in good agreement with the value found for HDA ice prepared at much higher pressures (Mishima *et al.*, 1984; Tulk *et al.*, 2002). The peak position shifts only slightly at temperatures up to 130 K. However, between 130 and 140 K, the peak shifts from 2.08 Å^{-1} (d = 3.02 Å) at 130 K to 1.77 Å^{-1} (d = 3.55 Å) at 140 K. As seen in Fig. 2(*a*), the peak at 135 K is considerably broadened. The observed peak width is consistent with phase coexistence of HDA and LDA ice within the sample (Klotz *et al.*, 2005). Note that distinct intermediate states of amorphous ice have been reported with relaxation times of the order of many hours (Tulk *et al.*, 2002). These states are not observed distinctly in this case if they are present, since the temperature

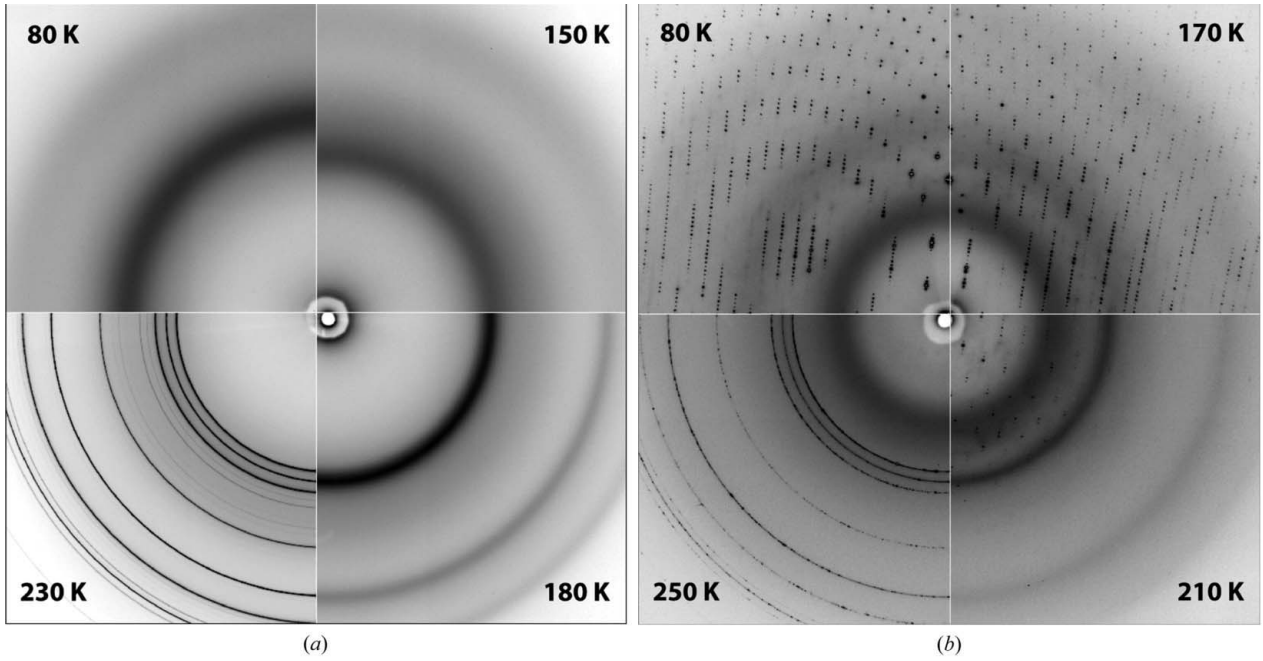

Figure 1
(*a*) X-ray diffraction images of the high-pressure cryocooled crystallization solution at different temperatures. The peak positions of amorphous ices at 80 K and 150 K are clearly distinguishable, indicating the density difference between HDA ice and LDA ice. The diffraction peaks of cubic ice and hexagonal ice are shown at 180 and 230 K, respectively. Note that the peak position at 150 K, which is at around 3.65 Å, matches the positions of the main sharp peaks at 180 and 230 K. The diffraction at 230 K includes diffraction from a small quantity of type I hydrate, presumably formed from the tartrate. (*b*) X-ray diffraction images of the high-pressure cryocooled thaumatin crystal at different temperatures. Crystal diffraction spots are seen superimposed on diffuse rings. These diffuse rings are due to oil (innermost ring) around the crystal and ice (second ring) inside the crystal. The broad ice peak is located at the Q value of 2.03 Å^{-1} (d = 3.10 Å) at 80 K, confirming that HDA ice formed inside the crystal by high-pressure cryocooling. The HDA ice transformed into LDA ice, cubic ice and hexagonal ice upon crystal warming. Note that the innermost diffraction ring from the oil changes little as the temperature is raised.

was increased much more quickly in this study. From 140 to 170 K, the peak position shifts toward the bulk LDA ice value of 1.71 Å^{-1} (d = 3.67 Å) (Dowell & Rinfret, 1960) and narrows in width to that expected for LDA ice.

Note that the sample consisted of 0.9 M sodium potassium tartrate as a protein crystallization agent. It was observed that the high-pressure cryocooling of pure water resulted in crystalline ice. This means that the solutes in the crystallization solution facilitated formation of the amorphous phase, likely by perturbing homogeneous nucleation (Kanno & Angell, 1977; Kanno, 1987). However, the X-ray scattering profiles of the crystallization solution still reflect the characteristic features of the HDA ice phase of pure water. The observed peak position and the shape of the scattering profile of the crystallization solution at approximately 80–130 K are consistent with the reported scattering from HDA ice formed from pure water (Mishima *et al.*, 1984, 1985; Bosio *et al.*, 1986). Since the peak position of the diffuse scattering is given by the inter-oxygen spacing of the scattering water, the amorphous ice phase formed in the crystallization solution is at a similar density to that of HDA ice of pure water. Beyond ∼140 K, the diffraction begins to exhibit the characteristic peaks of LDA ice located at around 1.71 Å^{-1} (d = 3.67 Å), a value typical of LDA ice (Dowell & Rinfret, 1960), indicating that the phase transition from HDA ice to LDA ice occurred as observed in pure water (Mishima *et al.*, 1984, 1985).

As temperature increased further, additional ice phases emerged (Figs. 1*a* and 2*a*). Between 165 and 170 K, somewhat sharper peaks began to appear in the distance ratio $3^{1/2}:8^{1/2}:11^{1/2}$, indicative of cubic ice (Blackman & Lisgarten, 1957). These peaks are much broader than those typical of crystalline phases, indicating microcrystalline ice. An analysis of the peak widths using the Scherrer equation suggests a crystallite size of 170 Å. The broad cubic ice lines became slightly sharper and eventually transformed to hexagonal ice around 210 K. Upon the phase transformation, the diffraction peaks became noticeably sharper with peak widths limited by the size of the X-ray beam. One can place a lower limit of 3000 Å on the domain size of the crystalline ice. Fig. 1(*a*)

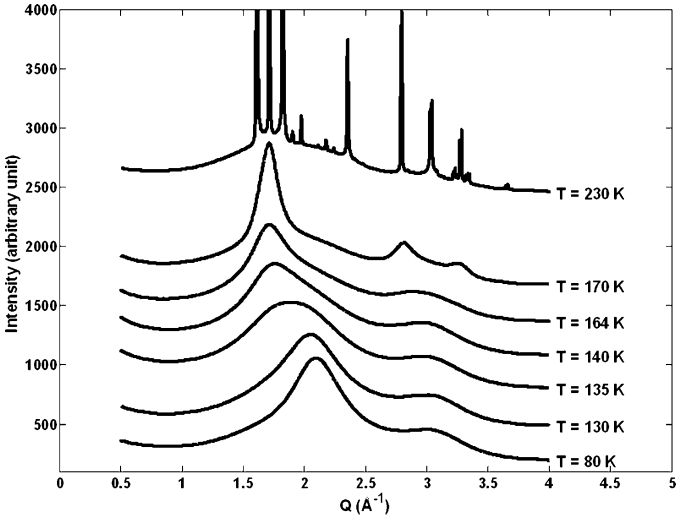

Figure 2
(*a*) X-ray diffraction intensity profiles of the high-pressure cryocooled crystallization solution upon warming. The profiles show the features characteristic of HDA ice in the 80 and 130 K curves, with a broad peak located at around 2.1 Å^{-1} (d = 3.0 Å). A significant change in the diffraction has occurred by 140 K, indicative of a phase transition from HDA to LDA ice. Around 170 K, the sample starts to crystallize and transform into cubic ice and finally to hexagonal ice at 230 K. (*b*) Median-filtered (to remove the sharp protein Bragg spots) X-ray diffraction intensity profiles of a high-pressure cryocooled thaumatin crystal upon warming. The scattering peak near 1.1 Å^{-1} (d = 5.7 Å) is due to oil coating the crystal. The second peak moves from 2.03 Å^{-1} (d = 3.10 Å) at 80 K to 1.72 Å^{-1} (d = 3.65 Å) at 170 K, indicating a transformation from HDA to LDA ice. The broad phase transition is indicative of confined water as opposed to the sharp transition seen for the bulk sample in (*a*).

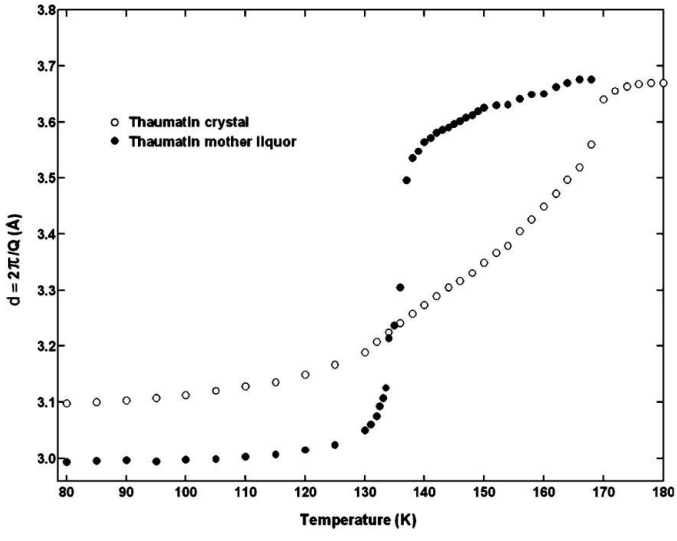

Figure 3
Ice peak position of the thaumatin crystallization solution (closed circles) and thaumatin crystal (open circles) prepared by high-pressure cryocooling. The position of the scattering from the solution shows a dramatic shift between 130 and 140 K, indicative of a phase transition from HDA ice to LDA ice. Above 170 K, the solution has transformed to cubic ice. The scattering from water within the crystal is located at higher d at low temperatures, and shows a wider phase transition between 130 and 170 K. This implies that the water inside the crystal behaves differently from bulk water because of its local environment and confined geometry.

shows the representative diffraction patterns of each crystalline ice phase: cubic ice at 180 K and hexagonal ice at 230 K, respectively. Note that the peak scattering position of LDA ice at around 1.71 Å^{-1} (d = 3.67 Å) is located at the position of the main crystalline diffraction peaks of cubic and hexagonal ice, consistent with the fact that crystalline ice and LDA ice have comparable densities (Ghormley & Hochanadel, 1971). The peak of the HDA ice scattering at 80 K in Fig. 1(*a*) is at a distinctly larger scattering angle. This indicates a smaller water–water distance and, hence, a higher density.

From 205 K (at the upper end of the cubic ice regime) to 230 K (into the hexagonal ice phase), peaks indicative of a type I gas hydrate (clathrate) are present (space group $Pm3n$, a = 11.83 Å) (Pauling & Marsh, 1952). We assume this is a clathrate of sodium potassium tartrate since no type I hydrate has been observed with helium (Londono *et al.*, 1992). In addition, given the rough stoichiometry of the type I clathrate, roughly 10% of the water would be needed to cage the tartrate. Indeed, the diffraction from the ice phase is an order of magnitude more intense. Note that this phase is not seen at 250 K, with only hexagonal ice present.

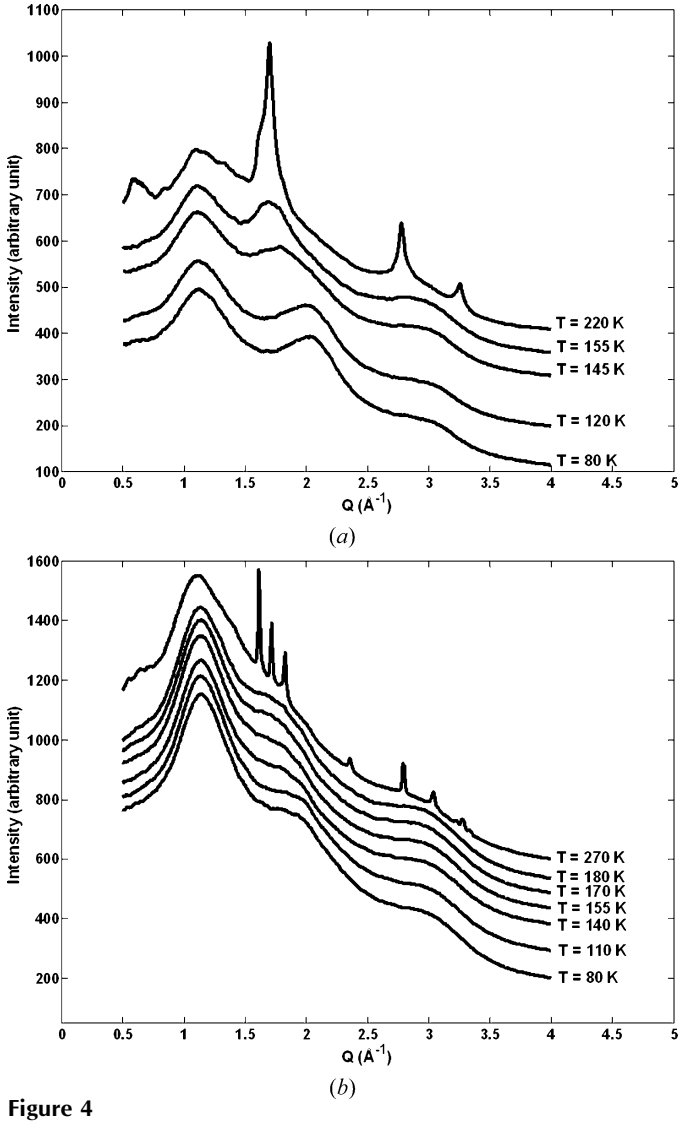

Figure 4
Median-filtered X-ray diffraction profiles of (*a*) glucose isomerase and (*b*) elastase crystals upon warming. The scattering peak near 1.1 Å^{-1} (d = 5.7 Å) is due to oil surrounding the crystal. The second peak is due to water within the crystal and shows a position indicative of HDA ice at low temperatures. Both peaks shift to lower Q at higher temperature, indicating a transition to LDA ice.

3.2. High-pressure cryocooled protein crystals

Fig. 1(*b*) shows the diffraction images of the high-pressure cryocooled thaumatin crystal at four different temperatures: 80, 170, 210 and 250 K. The scattering underlying the Bragg diffraction is due to the ice within the crystal plus the oil surrounding the crystal and is shown in Fig. 2(*b*). Upon warming, the solvent inside the high-pressure cryocooled crystal showed the characteristic diffraction peaks of all the ice phases observed in the bulk crystallization solution study. The position of the scattering peak due to the ice is plotted from 80 to 180 K in Fig. 3. At 80 K, the ice peak was located at Q = 2.03 Å^{-1} (d = 3.10 Å). This indicates an ice density well above that of LDA ice and near that of the HDA phase in bulk solution. A phase transition from HDA ice to LDA ice was observed between 130 and 170 K. The peak position (Q = 1.73 Å^{-1}, d = 3.63 Å) of the LDA ice inside the high-pressure cryocooled thaumatin crystal at 168 K was comparable with that (Q = 1.79 Å^{-1}, d = 3.51 Å) of the LDA ice at 80 K from a thaumatin crystal cryocooled at ambient pressure with 20%(*v*/*v*) glycerol. Note that the phase transition occurred over a wide temperature range, indicating that the scattering arises from water confined within the protein crystal unit cell or within small inclusions between crystalline mosaic blocks rather than from bulk water. One expects this confined water to behave differently from bulk water due to its local environment and confined geometry (Mayer, 1994).

Above 170 K, cubic ice began to form. As with the bulk solution sample, the peak widths indicate small crystalline ice domains of the order of 160 Å in size. Note that this domain size is of the order of the unit-cell size of the protein (thaumatin space group of $P4_12_12$, having $a = b \simeq 58$ Å and $c \simeq 150$ Å). In addition to the cubic ice, there appears to be a weak amorphous scattering peak remaining under the cubic ice peak. Due to the presence of the larger oil scattering peak and the uncertainties in its line shape, however, it is not possible to give an accurate measure of the scattering intensity of this amorphous peak. As the temperature is increased further, hexagonal ice is formed with the ice domain size greater than 3000 Å, along with further reduction in the amorphous water scattering peak. Note that no clathrate diffraction was observed with the protein crystal. Since the bulk solution was removed before freezing, no free tartrate remained in the sample to form the clathrate.

During crystal warming, we noticed that the quality of crystal diffraction from the protein was correlated with the ice phase of the water inside the crystal as seen in Fig. 1(*b*). Upon transition from HDA ice to LDA ice, the resolution limit of crystal diffraction slightly decreased and the crystal mosaicity increased by ∼130% (from 0.27° at 130 K to 0.62° at 170 K). This result seems reasonable given that ice expands by ∼24%

in volume during the phase transition from HDA (density of 1.17 g cm^{-3}) to LDA ice (density of 0.94 g cm^{-3}) which can lead to disruption of the crystal. Since the thaumatin crystal consists of ~55% solvent, the simplest estimate would yield a roughly 13% increase in the unit-cell volume upon the formation of LDA ice. Interestingly, however, only a 2.5% unit-cell volume expansion was observed from 130 to 170 K. Furthermore, in the temperature range of 80–200 K, the unit-cell volume was linear with temperature with little change in slope, even during the HDA to LDA ice phase transition. While this is less than the simple estimate, it is five times greater than the unit-cell expansion observed for a crystal flash-frozen at ambient pressure then warmed over the same temperature range, indicating that the effects of the high-pressure cryocooling are being released in a continuous fashion as the crystal is warmed. Similar behavior has also been reported in protein crystals that were high-pressure frozen within liquid pentane (Urayama, 2001).

The estimate of 13% volume change assumes that the ice retains the properties of bulk water and that all the water remains in the unit cell. The packing of water in the hydration shell around the protein is highly disrupted from the bulk state and will reduce the amount of water that undergoes the full volume change at the phase transition. Furthermore, the number of water molecules within the unit cell does not have to remain constant with temperature. As water is excluded from the unit cell, it can gather into inclusions between the mosaic blocks of the protein crystal. Changes in this inclusion neighborhood can affect the mosaicity without changing the volume of the unit cell. The total fraction of water in these inclusions is difficult to estimate, although we know from the broad phase transition that most of the water begins in highly confined surroundings. Furthermore, we know that the scattering from water in the cubic and hexagonal ice phases comes from domains that are too large to fit within the unit cell of the protein. While the cubic phase domains are quite small, the ice domains have been refined to considerable size in the hexagonal phase. Each of these implies that considerable water migration is occurring within the crystal even at low temperatures.

Upon formation of crystalline cubic ice from LDA ice, the crystal diffraction from the protein became even more degraded, with a continuous reduction in the resolution limit as the crystal warmed through the cubic ice region. Interestingly, the mosaic spread of the crystal is roughly the same as for the LDA ice phase. The protein crystal diffraction entirely disappeared upon the formation of hexagonal ice. We calculated that the total absorbed dose for the high-pressure cryocooled crystal up to the formation of hexagonal ice is about 10^7 Gy, which is less than the Henderson dose limit of 2×10^7 Gy (Henderson, 1990), where a crystal loses roughly half of its diffraction power. Furthermore, it was observed that crystal diffraction degraded by similar amounts during the crystalline ice formation for thaumatin crystals irradiated by considerably different X-ray doses. Therefore, we conclude that the crystal degradation is mostly due to the formation of crystalline ice, not radiation damage. This observation is somewhat unexpected based on the previously proposed mechanism for the crystal damage upon cooling involving solvent volume expansion (Kriminski *et al.*, 2002; Juers & Matthews, 2004), because the volume expansion during the formation of cubic or hexagonal ice from LDA ice is negligible (Ghormley & Hochanadel, 1971). It is likely that water initially associated within the unit cell of the high-pressure cryocooled sample is expelled upon the formation of LDA ice and becomes refined into sequentially larger ice domains included among the protein crystal mosaic blocks upon the formation of cubic and hexagonal ice, which seems to lead to a drastic degradation of the crystal diffraction. The microcrystal size of the crystalline ice (about 160 Å for cubic ice and greater than 3000 Å for hexagonal ice) supports this hypothesis. However, revealing the detailed mechanism of crystal disruption during the growth of the crystalline ice domain is beyond the scope of this paper.

The formation of HDA ice within other protein crystal systems by high-pressure cryocooling was also investigated. The underlying diffuse scattering profiles from glucose isomerase and elastase crystals are shown in Figs. 4(*a*) and 4(*b*), respectively. Phase transitions from HDA ice to LDA ice, cubic ice and hexagonal ice were observed in these protein crystals as well. Interestingly, the phase transition from HDA to LDA ice was observed between 130 and 155 K for glucose isomerase, which is sharper than for thaumatin. At 80 K, the glucose isomerase crystal showed an ice scattering peak at 2.04 Å^{-1} (d = 3.08 Å) whereas the elastase crystal showed scattering at 1.84 Å^{-1} (d = 3.41 Å). While the glucose isomerase value is near that of the bulk HDA value, the value from elastase indicates an intermediate density with respect the to HDA and LDA ice phases. The elastase has the lowest solvent content of any of the crystals studied. One would expect the water in this crystal to be the most constrained, and hence, the most perturbed from the bulk HDA value. While the formation of HDA ice appears to be a general feature of high-pressure cryocooling, the degree to which the water is free to arrange seems to be a function of the solvent content. As in the case of the high-pressure cryocooled thaumatin crystal, the crystal diffraction of glucose isomerase and elastase was slightly degraded during the phase transition from HDA ice to LDA ice and drastically deteriorated upon the formation of cubic and hexagonal ice. This observation confirms that the quality of crystal diffraction is closely related to the ice phase inside the protein crystal, independent of the protein.

4. Conclusions

It has been demonstrated that high-pressure cryocooling induces HDA ice both in a bulk solution used in protein crystallization and in the water included within protein crystals. X-ray diffraction studies clearly showed features characteristic of amorphous ice at densities near those of HDA ice at low temperatures. Upon warming of the high-pressure cryocooled crystallization solution, phase transitions from HDA ice to LDA ice, cubic ice and hexagonal ice could be

clearly observed. The same phase transitions were observed in the high-pressure cryocooled protein crystals. The ice phases were closely related to the diffraction quality of the crystals. This observation supports the proposed mechanism of high-pressure cryocooling.

Our results may have implications for the biological applications of the method and its technical modification for high-throughput crystallography. As suggested by Kim *et al.* (2007), high-pressure cryocooling in capillaries opens novel routes for high-throughput protein crystallography. High-pressure cryocooling at up to 200 MPa of pure water in capillaries always resulted in crystalline ice (data not shown). In the case of the thaumatin crystallization solution, the salts in the solution appear sufficient to prevent ice crystal formation upon high-pressure cryocooling. Similarly, relatively low concentrations of glycerol and other common cryoprotectants were successfully high-pressure cryocooled in capillaries. This suggests a straightforward strategy for the preparation of high-pressure cryocooled protein crystals in capillaries: identify minimum concentrations of relatively innocuous cryoprotectant solutions that yield HDA when high-pressure cryocooled in capillaries; these may then be added to the mother liquor used to crystallize proteins. In this way, one is assured that the protein crystals may be high-pressure cryocooled in their crystallization solutions.

We thank the MacCHESS staff for assistance in data collection, Buz Barstow, Nozomi Ando and Gil Toombes for useful comments, and George T. DeTitta, Michael G. Malkowski and Edward H. Snell for encouragement. This work was supported by US NIH grant GM074899, the MacCHESS grant (US NIH grant RR001646), by US DOE grant DE-FG02-97ER62443, and CHESS, which is supported by the US NSF and NIH-NIGMS through NSF grant DMR-0225180.

References

Albright, R. A., Vazquez Ibar, J.-L., Kim, C. U., Gruner, S. M. & Morais Cabral, J. H. (2006). *Cell*, **126**, 1147–1159.
Blackman, M. & Lisgarten, N. D. (1957). *Proc. R. Soc. London Ser. A*, **239**, 93–107.
Bosio, L., Johari, G. P. & Teixeira, J. (1986). *Phys. Rev. Lett.* **56**, 460–463.
Carrell, H. L., Glusker, J. P., Burger, V., Manfre, F., Tritsch, D. & Biellmann, J.-F. (1989). *Proc. Natl Acad. Sci. USA*, **86**, 4440–4444.
Dowell, L. G. & Rinfret, A. P. (1960). *Nature (London)*, **188**, 1144–1148.
Garman, E. F. & Owen, R. L. (2006). *Acta Cryst.* D**62**, 32–47.
Garman, E. F. & Schneider, T. R. (1997). *J. Appl. Cryst.* **30**, 211–237.
Ghormley, J. A. & Hochanadel, C. J. (1971). *Science*, **171**, 62–64.
Henderson, R. (1990). *Proc. R. Soc. London Ser. B*, **241**, 6–8.
Juers, D. H. & Matthews, B. W. (2004). *Q. Rev. Biophys.* **37**, 1–15.
Kanno, H. (1987). *J. Phys. Chem.* **91**, 1967–1971.
Kanno, H. & Angell, C. A. (1977). *J. Phys. Chem.* **81**, 2639–2643.
Kim, C. U., Hao, Q. & Gruner, S. M. (2006). *Acta Cryst.* D**62**, 687–694.
Kim, C. U., Hao, Q. & Gruner, S. M. (2007). *Acta Cryst.* D**63**, 653–659.
Kim, C. U., Kapfer, R. & Gruner, S. M. (2005). *Acta Cryst.* D**61**, 881–890.
Klotz, S., Strässle, Th., Nelmes, R. J., Loveday, J. S., Hamel, G., Rousse, G., Canny, B., Chervin, J. C. & Saitta, A. M. (2005). *Phys. Rev. Lett.* **94**, 025506.
Ko, T.-P., Day, J., Greenwood, A. & McPherson, A. (1994). *Acta Cryst.* D**50**, 813–825.
Kriminski, S., Caylor, C. L., Nonato, M. C., Finkelstein, K. D. & Thorne, R. E. (2002). *Acta Cryst.* D**58**, 459–471.
Londono, D., Finney, J. L. & Kuhs, W. F. (1992). *J. Chem. Phys.* **97**, 547–552.
Mayer, E. (1994). *Hydrogen Bonded Networks*, edited by M.-C. Bellissent-Funel & J. C. Dore, pp. 355–372. Dordrecht: Kluwer Academic Publishers.
Mishima, O., Calvert, L. D. & Whalley, E. (1984). *Nature (London)*, **310**, 393–395.
Mishima, O., Calvert, L. D. & Whalley, E. (1985). *Nature (London)*, **314**, 76–78.
Mishima, O. & Stanley, H. E. (1998). *Nature (London)*, **396**, 329–335.
Otwinowski, Z. & Minor, W. (1997). *Methods Enzymol.* **276**, 307–326.
Pauling, L. & Marsh, R. E. (1952). *Proc. Natl. Acad. Sci. USA*, **38**, 112–118.
Ravelli, R. B. & Garman, E. F. (2006). *Curr. Opin. Struct. Biol.* **16**, 624–629.
Shotton, D. M., Hartley, B. S., Camerman, N., Hofman, T., Nyburg, S. C. & Rao, L. (1968). *J. Mol. Biol.* **32**, 155–156.
Tulk, C. A., Benmore, C. J., Urquidi, J., Klug, D. D., Neuefeind, J., Tomberli, B. & Egelstaff, P. A. (2002). *Science*, **297**, 1320–1323.
Urayama, P. (2001). PhD thesis, Cornell University, USA.